

# Synthesis of Fe<sub>3</sub>O<sub>4</sub>/ZnO/CuO Nanocomposite and Its Sono-Photocatalyst Property for Removal of Methylene Blue from Wastewater

Samira Pishkar Ahrab<sup>1</sup>, Mahdiyeh Pourali<sup>2</sup>, MohammadTaghi Hamedani<sup>1,\*</sup>

\* *m.hamedani.tabrizu@gmail.com*

<sup>1</sup> Faculty of Mechanical Engineering, Tabriz University, Tabriz, 51616471, Iran

<sup>2</sup> Faculty of Materials Engineering, Sahand University of Technology, Tabriz, 513351996, Iran

Received: April 2025

Revised: November 2025

Accepted: December 2025

DOI: 10.22068/ijmse.4019

**Abstract:** Fe<sub>3</sub>O<sub>4</sub>/ZnO/CuO nanocomposites with various molar ratios of CuO were successfully synthesized. The sol-gel method was used to synthesise nanocomposite materials at low temperature. A set of experiments, including X-ray diffraction (XRD), Dynamic Light Scattering (DLS), scanning electron microscopy (SEM), and UV-Vis spectroscopy, were used to confirm the successful synthesis of Fe<sub>3</sub>O<sub>4</sub>/ZnO/CuO nanocomposites in crystalline form. The photocatalytic activity of the samples was investigated via the degradation of the methylene blue (MB) dye from synthetic wastewater under three distinct conditions: visible light, ultraviolet light, and a combination of visible light with ultrasonic treatment. The Fe<sub>3</sub>O<sub>4</sub>/ZnO/CuO nanocomposite with a 1:1:0.5 molar ratio exhibited the highest photocatalytic activity under both visible and ultraviolet irradiation. Furthermore, when visible light was combined with ultrasonic treatment, complete (100%) removal of methylene blue was achieved within 120 minutes. The results demonstrate that these nanocomposites are efficient catalysts for wastewater treatment, removing organic pollutants.

**Keywords:** Fe<sub>3</sub>O<sub>4</sub>/ZnO/CuO, Sono-photocatalyst, Nanocomposite, Wastewater treatment.

## 1. INTRODUCTION

Over the past few decades, emerging problems in the industry have attracted significant attention worldwide, particularly environmental pollution [1]. The release of organic dyes from the textile, leather, food, cosmetics, and pharmaceutical industries into the environment has caused significant problems for living organisms. Also, water pollution is a problem that should be identified promptly. Researchers have conducted extensive research on how to treat wastewater from the processing of industrial products and household waste [2]. Nevertheless, the conventional wastewater treatment method still contains a large number of contaminants that are challenging to eliminate.

For instance, antibiotics, dyes, organic insecticides, multi-rheological aromatic hydrocarbons [3-6], etc. New techniques, such as Fenton oxidation [7] and hybrid approaches combining multiple purification processes, such as active carbon, biofilm, and enzymatic reactors, have been developed to remove these contaminants [8]. These techniques have attracted the attention of researchers [9] and have a positive impact on the degradation of contaminated organic matter. Another method for removing pollutants is to use Semiconducting oxides with photocatalytic properties. Various catalysts have been introduced to remove pollutants or convert

them into non-irritating chemicals [10]. Among them, TiO<sub>2</sub> and ZnO semiconductors have been shown to be effective photocatalysts for the destruction of organic pollutants. The advantages of ZnO nanoparticles include strong oxidising ability, light sensitivity, excellent mechanical and chemical stability, non-toxicity, a favourable energy gap, and a low price [11]. However, to use ZnO as a photocatalyst, given its band gap (3.2 electron volts), it requires ultraviolet light, which accounts for only about 10% of sunlight. In sunlight, 45% of the radiation falls within the visible range [12, 13]. To enhance the photocatalytic activity of ZnO under visible light, solutions need to be considered. The formation of a ZnO nanoparticle composite with other metal oxides results in stronger visible-light absorption [14]. In addition, this composite prevents recombination of electron-hole and increases the photocatalyst's efficiency [15]. The coupling of ZnO with CuO nanoparticles and the formation of a composite are promising approaches for enhancing photocatalytic properties. Besides extending the absorption range towards the visible light, this method transmits electrons produced by the photon from a high-conductivity band of CuO to a low-conductivity band of ZnO, which results in the effective separation of the electron-hole [16]. So far, considerable research has been conducted on the synthesis of ZnO/CuO

as a high-level catalyst. A number of techniques have been used to create a ZnO/CuO catalyst, including mechanical methods (e.g., grinding), wet chemistry, coprecipitation, thermal decomposition, sol-gel, hydrothermal, and photo deposition [17]. Another problem for catalysts is their tendency to segregate from purified water in practical applications. Traditional methods such as coagulation and filtration degrade catalysts and increase energy consumption [18]. Using an external magnet, researchers have recently paired magnetic nanoparticles with photocatalytically active materials to improve catalyst separation and recycling [19]. Therefore, the introduction of magnetic materials, such as Fe<sub>3</sub>O<sub>4</sub>, into Fe<sub>3</sub>O<sub>4</sub>/ZnO/CuO nanocomposites simplifies magnetic separation. Nanocatalysts are beneficial for academic and industrial research due to their high reaction rates, perfect activation of adsorbed compounds, ease of use, high selectivity, recyclability, and eco-friendliness. Because of their appealing features, nanometal oxides have been utilized as solid catalysts in a variety of organic processes [20]. In explaining the photocatalytic effect, it can be said that in the absence of degradation matter, hydro-carbons often decompose slowly. The photocatalyst reduces the activation energy of the decomposition reaction, thereby accelerating the reaction. As a result of light collisions with photocatalytic materials, electron holes are generated, leading to high oxidation and resuscitation [21]. Nowadays, the use of ultrasonics in the presence of a catalyst (sonocatalytic decomposition) is an eco-friendly method for removing dyes from wastewater. The influence of ultrasonic waves is the heat produced by a hole explosion, which converts water molecules into hydroxyl radicals and reactive hydrogen atoms. Both species can react with organic dyes, leading to the breakdown and elimination of various contaminants from wastewater [22]. As a result, the simultaneous use of light and ultrasonic radiation to analyze different colors has been investigated [19-22]. In the current study, the impact of light and ultrasound irradiation, as well as the metal oxide content, on the photocatalytic activity of the Fe<sub>3</sub>O<sub>4</sub>/ZnO/CuO nanocomposites has been investigated. The optical and morphological analyses were followed by a photocatalytic activity test for methylene blue (MB) degradation in wastewater.

## 2. EXPERIMENTAL PROCEDURES

In this study, iron (II) sulfate heptahydrate (FeSO<sub>4</sub>·7H<sub>2</sub>O,

99%), copper sulfate pentahydrate (CuSO<sub>4</sub>·5H<sub>2</sub>O, 99%), zinc sulfate heptahydrate (ZnSO<sub>4</sub>·7H<sub>2</sub>O, 99%) and sodium hydroxide (NaOH) (Merck Company) were used as raw materials.

CuO and Fe<sub>3</sub>O<sub>4</sub> nanoparticles were synthesized using the sol-gel method. In this method, 0.025 mole of CuSO<sub>4</sub>·5H<sub>2</sub>O was dissolved in 100 mL of deionized water with constant magnetic stirring. Then 0.05 mole of NaOH was dissolved in 150 mL of deionised water and added to the solution in droplets to achieve the desired pH. The solution was then heated to 80°C for 3 hours to form the gel. After 4 hours, the black product was dissolved using filter paper and then dried at 80°C for 4 hours in an oven to obtain Copper oxide nanoparticles.

To obtain Fe<sub>3</sub>O<sub>4</sub> nanoparticles, 0.027 mole of FeSO<sub>4</sub>·7H<sub>2</sub>O, was dissolved in 100 mL of deionized water and continuously stirred at room temperature. To control the pH to 3, acetic acid (CH<sub>3</sub>COOH) and 30 mL of ethylene glycol (EG), both in pure form, were added to the solution. Then, 0.054 mole of NaOH was dissolved in 150 mL of deionized water and added dropwise to the mixture. The final solution was stirred at 80°C for 3 h to form a gel. The gel was dried at 80°C for 4 h.

To synthesize the Fe<sub>3</sub>O<sub>4</sub>/ZnO/CuO nanocomposite, 0.0125 mole of ZnSO<sub>4</sub>·7H<sub>2</sub>O was dissolved in 30 mL of distilled water under magnetic stirring. Then, 0.025 mole of NaOH in 65 mL of deionized water was added to the solution in droplets to reach the appropriate pH, which was then stirred and heated to 80°C. The previously synthesized Fe<sub>3</sub>O<sub>4</sub> and CuO nanoparticles were dispersed in 30 mL of ethanol (99.7%) and then added to the initial solution. The resulting mixture was continuously stirred at 80°C for 2 hours. Finally, ZnO was formed in situ on the surface of the pre-formed Fe<sub>3</sub>O<sub>4</sub> and CuO. At the end, the product was isolated using filter paper and washed several times with distilled water and ethanol to remove impurities. The final product was left at room temperature overnight, then dried at 100°C for 1 hour. Nanocomposite Fe<sub>3</sub>O<sub>4</sub>/ZnO/CuO with the molar ratios of (1:1:0.3, 1:1:0.5, 1:1:1, 1:1:3) was prepared by changing the concentrations of the precursor solutions and evaluated.

X-ray diffraction peaks were measured by an XRD analyzer (Siemens D5000 X-ray diffractometer). The analysis was conducted under Cu- $\alpha$  radiation ( $\lambda = 1.54178 \text{ \AA}$ ), a scanning rate of 20°/min, a  $2\theta$  range of 20–80°, and operating conditions of 30 kV and 40 mA. Also, Crystallite size is estimated by

Scherer's equation (Eq. 1) [23]:

$$D = 0.9\lambda / \beta \cos\Theta \quad (\text{Eq. 1})$$

where  $D$  is the size of the crystals in nanometers,  $\beta$  is the peak width at half the maximum intensity in radians in radian,  $\lambda$  is the x-ray wavelength in nanometers, and  $\Theta$  is the Bragg angle corresponding to the diffraction peak.

SEM (Stereo Scan 360) was performed to verify the morphology of the nanoparticles. Elemental analysis of the samples was performed using X-ray diffraction spectroscopy (EDX). A dot map was used to determine the distribution of the elements in the nanocomposite. To investigate particle size distribution by DLS, Nanotracer Wave of Microtrac Co. was used and to determine the adsorption edge and band gap of synthesized zinc oxide and prepared nanocomposites, DRS spectroscopic analysis was performed. The absorption wavelength was obtained by extrapolating the linear portion of the absorption intensity curve.

Eq. 2 was used to calculate the band gap [24]:

$$E_g = hc / \lambda_g \quad (\text{Eq. 2})$$

In this respect,  $E_g$  is the band gap in electron volts,  $h$  is the Planck constant, which equals  $4.13567 \times 10^{-15}$  eV,  $c$  is the light speed, which equals 299792458 m/s, and  $\lambda_g$  is the absorption wavelength.

The effectiveness of the photocatalysts was tested by measuring their ability to break down methylene blue (MB) in 100 mL beakers. In this test, the Philips 9W UV-C lamp was used as the UV light source, and the 120-watt metal halide lamp was used as the visible light source. Photocatalytic test equipment was mounted and sealed in a dark chamber to prevent radiation loss. For the determination of photocatalytic activity, 0.05 g of the nanocomposite samples was dispersed in 100 mL of MB solution at a concentration of 0.005 g/L using a magnetic stirrer.

Before illumination, the reaction mixture was kept in dark conditions for 20 minutes to establish adsorption-desorption equilibrium. After collecting the initial sample, the photocatalytic reaction was initiated by activating the light source. Subsequent samples were collected at 20-minute intervals (20, 40, 60, 80, 100, and 120 minutes), and each sample was analysed by UV-Vis spectroscopy. The concentration of Methylene Blue (MB) was determined by measuring the UV-Vis absorbance at its characteristic peak wavelength of 665 nm. A calibration curve was created and used to convert the measured absorbance values into actual dye

concentrations. The degradation rate was then determined using the following equation [25]:

$$(I_0 - I_t) / I_0 \times 100 = (C_0 - C_t) / C_0 \times 100 \quad (\text{Eq. 3})$$

Where  $C$  represents the concentration of Methylene Blue (MB) at any given time during the reaction, while  $C_0$  is the initial MB concentration after reaching adsorption-desorption equilibrium, similarly,  $A$  represents the absorbance value measured at any point during the reaction, and  $A_0$  is the initial absorbance value recorded at equilibrium.

To evaluate how ultrasonic treatment affects photocatalytic activity,  $\text{Fe}_3\text{O}_4/\text{ZnO}/\text{CuO}$  nanocomposites (0.05 g) with varying molar ratios were dispersed in Methylene Blue solution (100 mL, 0.005 g/L) using ultrasonication and subjected to visible light irradiation for intervals of 20, 40, 60, 80, 100 and 120 minutes.

### 3. RESULTS AND DISCUSSION

The XRD patterns shown in Fig. 1 display the diffraction patterns of  $\text{Fe}_3\text{O}_4/\text{ZnO}/\text{CuO}$  nanocomposites synthesised at different CuO molar ratios. The patterns exhibit characteristic diffraction peaks corresponding to cubic spinel  $\text{Fe}_3\text{O}_4$ , monoclinic CuO, and hexagonal wurtzite ZnO structures. The absence of impurities or secondary phases in the patterns indicates that the  $\text{Fe}_3\text{O}_4/\text{ZnO}/\text{CuO}$  nanocomposites were successfully synthesised. All XRD peaks corresponding to [101] Planes related to hexagonal ZnO structure ( $2\Theta = 32.5$ ), [200] planes related to CuO monoclinic structure ( $2\Theta = 39.5$ ), and [311] planes for cubic spinel structure  $\text{Fe}_3\text{O}_4$  ( $2\Theta = 35.5$ ) have the highest growth rates. Furthermore, analysis of the XRD patterns for  $\text{Fe}_3\text{O}_4/\text{ZnO}/\text{CuO}$  nanocomposites with varying molar ratios reveals a clear trend: as the molar ratio of CuO to ZnO increases, there is a corresponding increase in the intensity of CuO diffraction peaks, while simultaneously showing a decrease in the intensity of both ZnO and  $\text{Fe}_3\text{O}_4$  diffraction peaks. Changes in the pattern intensity revealed an increase in CuO content within the nanocomposite structure.

In all XRD diagrams, based on peak positions, it can be seen that ZnO does not form a solid solution with CuO or  $\text{Fe}_3\text{O}_4$ , and the  $\text{Fe}_3\text{O}_4/\text{ZnO}/\text{CuO}$  nanocomposite is considered a nanocomposite powder of ZnO,  $\text{Fe}_3\text{O}_4$ , and CuO crystals.

Fig. 2 shows the XRD pattern of  $\text{Fe}_3\text{O}_4/\text{ZnO}/\text{CuO}$  nanocomposite with molar ratios of 1:1:0.3, 1:1:0.5, 1:1:1, and 1:1:3 for a,b,c, and d images,

respectively. According to reference data, 01-075-0033 demonstrated Fe<sub>3</sub>O<sub>4</sub> in the cubic phase, 0254-041-00 determined the hexagonal crystalline phase of ZnO, and 0704-076-01 demonstrated CuO with a monoclinic crystalline structure.

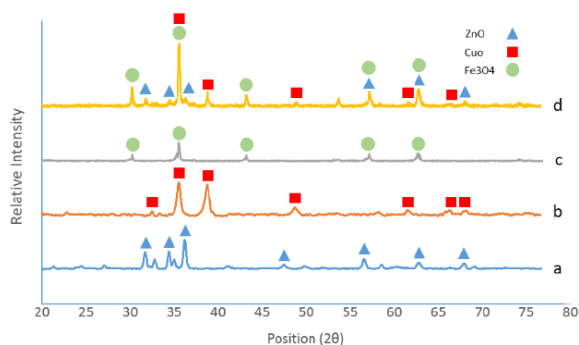


**Fig. 1.** XRD patterns of synthesized Fe<sub>3</sub>O<sub>4</sub>/ZnO/CuO nanocomposite: a) ZnO, b) CuO, c) Fe<sub>3</sub>O<sub>4</sub>, d) Fe<sub>3</sub>O<sub>4</sub>/ZnO/CuO nanocomposite

In the Table 1, the particle size of Fe<sub>3</sub>O<sub>4</sub>, ZnO, CuO, and Fe<sub>3</sub>O<sub>4</sub>/ZnO/CuO nanocomposites with molar ratios of 1:1:0.3, 1:1:0.5, 1: 1: 1 and 1: 1: 3 estimated by Scherrer's equation. By comparing the size of Fe<sub>3</sub>O<sub>4</sub>, ZnO, and CuO particles in Fe<sub>3</sub>O<sub>4</sub>/ZnO/CuO nanocomposites with different molar ratios, it is observed that the presence of CuO inhibits the growth of particles and reduces the size of ZnO and Fe<sub>3</sub>O<sub>4</sub> particles. In conclusion, CuO nanoparticles inhibit the growth of ZnO crystallites. It was evidenced by the significant reduction in ZnO crystallite size in the presence of CuO. In contrast, Fe<sub>3</sub>O<sub>4</sub> crystallite size shows a smaller decrease, indicating that CuO has a less pronounced effect on the growth of Fe<sub>3</sub>O<sub>4</sub> crystallites. The crystallite size of CuO varies with its concentration in the composites, highlighting its role in controlling crystallite growth.

Particle morphology of nanocomposites was investigated by scanning electron microscopy (SEM). Fig. 3 illustrates an SEM image of a Fe<sub>3</sub>O<sub>4</sub>/ZnO/CuO nanocomposite with a molar

ratio of 1:1:0.5. As shown in Fig. 3, the Fe<sub>3</sub>O<sub>4</sub>/ZnO/CuO nanocomposite is cauliflower-shaped. To compare the results, the size distributions of the conventional and synthesised catalysts were analysed using ImageJ. The analysis revealed that the synthesised samples had relatively small average particle sizes.

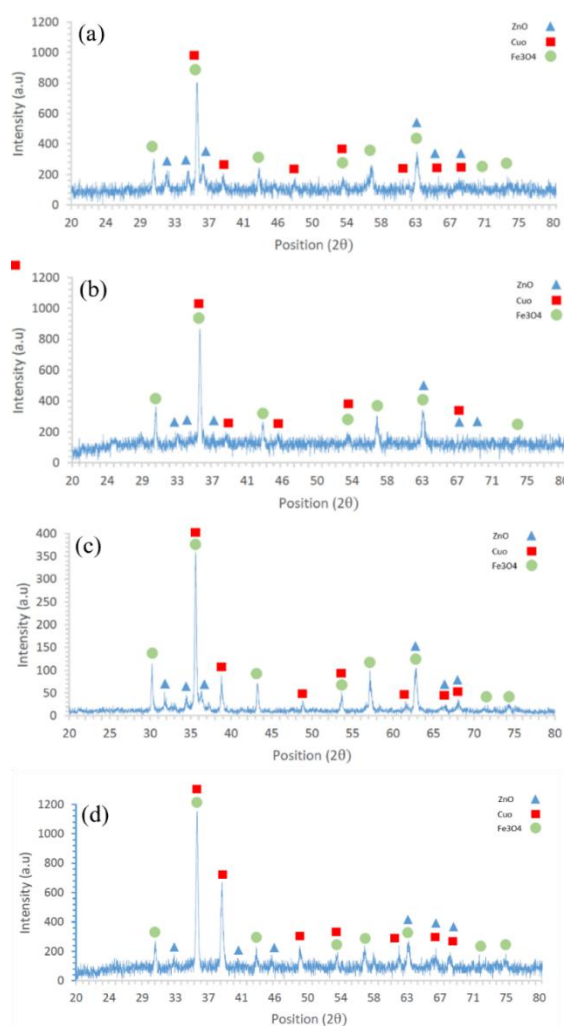


**Fig. 2.** XRD patterns of synthesized Fe<sub>3</sub>O<sub>4</sub>/ZnO/CuO nanocomposite: a) Fe<sub>3</sub>O<sub>4</sub>/ZnO/CuO (1:1:0.3), b) Fe<sub>3</sub>O<sub>4</sub>/ZnO/CuO (1:1:0.5), c) Fe<sub>3</sub>O<sub>4</sub>/ZnO/CuO (1:1:1) and d) Fe<sub>3</sub>O<sub>4</sub>/ZnO/CuO (1:1:3)

**Table 1.** Crystallite size of ZnO, CuO, and Fe<sub>3</sub>O<sub>4</sub> in Fe<sub>3</sub>O<sub>4</sub>/ZnO/CuO nanocomposite

Sample	ZnO crystallite size (nm)	CuO crystallite size (nm)	Fe <sub>3</sub> O <sub>4</sub> crystallite size (nm)
Fe <sub>3</sub> O <sub>4</sub>	-	-	44.5
CuO	-	19.31	-
ZnO	22.92	-	-
Fe <sub>3</sub> O <sub>4</sub> /ZnO/CuO (1:1:0.3)	19.21	20.15	44.01
Fe <sub>3</sub> O <sub>4</sub> /ZnO/CuO (1:1:0.5)	20.18	16.15	42.23
Fe <sub>3</sub> O <sub>4</sub> /ZnO/CuO (1:1:1)	19.65	18.62	41.15
Fe <sub>3</sub> O <sub>4</sub> /ZnO/CuO (1:1: 3)	17.15	21.48	40.15

This size distribution indicates the successful formation of nanostructured materials. Similar  $\text{Fe}_3\text{O}_4/\text{ZnO}/\text{CuO}$  morphologies have been reported in previous studies [20].

Above all, the numerous pores of different sizes within the 3D microstructure act as transport pathways for small molecules. This morphology and porosity provide a larger surface area for dye adsorption and catalytic reactions. The reduction in particle dimensions enhances the generation of electron-hole pairs when exposed to light, resulting in more effective degradation of contaminants during performance testing.

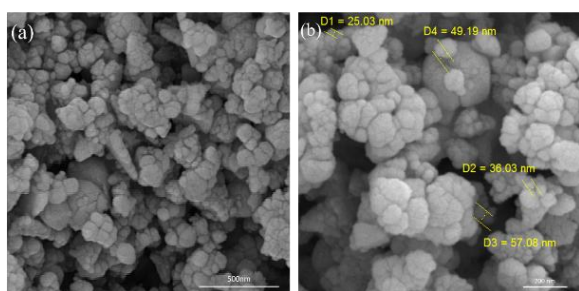


**Fig. 3.** SEM image of synthesized  $\text{Fe}_3\text{O}_4/\text{ZnO}/\text{CuO}$  nanocomposite, a) SEM Mag 70kx, b) SEM Mag 100kx Particle Size Distribution

EDX analysis aims to determine the distribution of elements on the catalyst surface. As shown in Fig. 4, the characteristic peaks of the elements of oxygen, iron, copper, and zinc indicate the presence of these elements in the nanocomposite structure. It should be noted that the samples had no impurities. The peak in the range of 1.8-2.2 keV is related to the gold element, which is coated on the nanocomposite in the SEM analysis, to provide conductivity in the sample. In Table 2, the weight and atomic percentages of the elements are specified, confirming the proper synthesis of the samples.

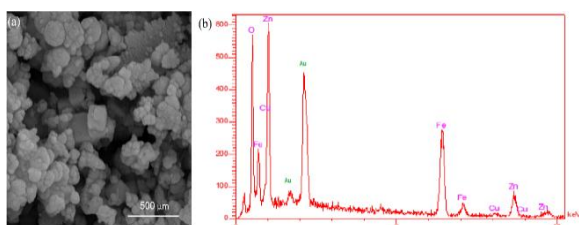


**Fig. 4.** EDX analysis of synthesized  $\text{Fe}_3\text{O}_4/\text{ZnO}/\text{CuO}$  nanocomposite: a) SEM image of the area selected for EDX analysis, b) EDX results in  $\text{Fe}_3\text{O}_4/\text{ZnO}/\text{CuO}$  nanocomposite (1:1:0.5)

To investigate the distribution of elements in the

photocatalyst structure, dot Map analysis was prepared from  $\text{Fe}_3\text{O}_4/\text{ZnO}/\text{CuO}$  nanocomposite (1:1:0.5) as shown in Fig. 5. The elemental distribution analysis of the photocatalyst structure was conducted on the selected region shown in Fig. 5a. Images 5b, 5c, 5d, and 5e show the distribution of copper, iron, zinc, and oxygen, respectively. Moreover, the elements are homogeneously distributed in the structure.

**Table 2.** Comparative amount of elements in the structure of  $\text{Fe}_3\text{O}_4/\text{ZnO}/\text{CuO}$  nanocomposite (1:1:0.5)

Sample	Weight percentage (%W)	Atomic percentage (%A)
$\text{O}_{K\alpha}$	28.77	60.03
$\text{Cu}_{K\alpha}$	1.72	0.9
$\text{Zn}_{K\alpha}$	28.38	14.49
$\text{Fe}_{K\alpha}$	41.12	24.57

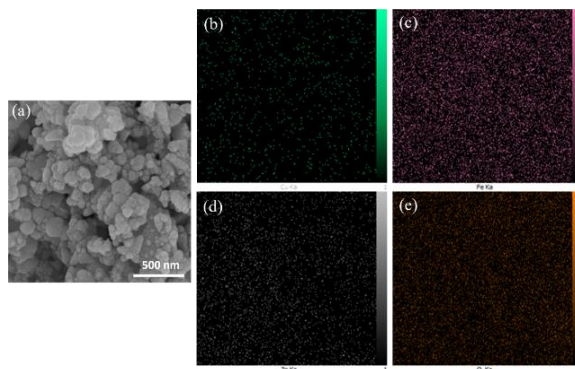


**Fig. 5.** Dot map analysis of synthesized  $\text{Fe}_3\text{O}_4/\text{ZnO}/\text{CuO}$  nanocomposite: a) Selected area for dot map analysis, b) Cu, c) Fe, d) Zn, e) O

In this study, the photocatalytic performance of  $\text{Fe}_3\text{O}_4/\text{ZnO}/\text{CuO}$  nanocomposites was investigated by analyzing the relationship between band gap and varying molar ratios of the components. The photocatalytic degradation efficiency of pollutants is primarily determined by the band gap, which serves as the critical parameter in the process. For this purpose, the absorption spectra of the nanocomposites were measured using a UV-visible spectrophotometer, and the results are shown in Fig. 6(a). The bandgap energies of the samples were determined using Tauc's plots by extrapolating the linear part of the plots to the  $h\nu$  axis, as shown in Fig. 6(b).

ZnO nanoparticles exhibit strong absorption in the wavelength range of 200-400 nm, and the absorption edge of the samples shifts to 372 nm with increasing copper oxide content in the visible

light region. Coupling zinc oxide with copper oxide narrows the band gap. This reduction in the band gap occurs because the addition of copper oxide to the nanocomposite introduces an intermediate energy band at the bottom of the zinc oxide conduction band. This interaction decreases the energy difference between the valence and conduction bands of zinc oxide, thereby reducing the overall band gap. According to the literature, ZnO nanoparticles are n-type semiconductors, whereas CuO nanoparticles are p-type. In this study, the photocatalytic performance was enhanced by creating a heterojunction between n-type and p-type semiconductors, while simultaneously studying how this junction influences the optical characteristics. In Table 3, the absorption wavelength and energy of the band gap region for each sample are calculated using the following equation:

$$(\alpha h\nu)^2 = A(h\nu - E_g) \quad (\text{Eq.4})$$

where  $\alpha$  is the absorption coefficient,  $h$  is Planck's constant,  $\nu$  is the photon frequency,  $E_g$  is the optical band gap, and  $A$  and  $n$  are constants. For the direct bandgap semiconductor,  $n = 2$ , and for the indirect transition bandgap,  $n = \frac{1}{2}$ . We assumed  $n = 2$  for our samples.

DLS analysis was performed to investigate particle size distribution. Fig. 7 illustrates the range of particle size distribution in the ZnO, Fe<sub>3</sub>O<sub>4</sub>/ZnO/CuO (1:1:0.3), Fe<sub>3</sub>O<sub>4</sub>/ZnO/CuO (1:1:0.5), Fe<sub>3</sub>O<sub>4</sub>/

ZnO/CuO (1:1:1), and Fe<sub>3</sub>O<sub>4</sub>/ZnO/CuO (1:1:3) samples, which are 486-1944, 486-6540, 25-409, 289-6540, 171.9-6540 nm, respectively.

On the other hand, the highest number of particles in the ZnO, Fe<sub>3</sub>O<sub>4</sub>/ZnO/CuO (1:1:0.3), Fe<sub>3</sub>O<sub>4</sub>/ZnO/CuO (1:1:0.5), Fe<sub>3</sub>O<sub>4</sub>/ZnO/CuO (1:1:1), and Fe<sub>3</sub>O<sub>4</sub>/ZnO/CuO (1:1:3) samples are 972, 687, 30.04, 289, and 171.9 nm, respectively. DLS measures the hydrodynamic diameter of particles (or agglomerates) in a solution, which is typically much larger than the primary particle size seen in SEM or the crystallite size from XRD. The results show that increasing the CuO content in the Fe<sub>3</sub>O<sub>4</sub>/ZnO/CuO nanocomposite does not consistently affect particle size. In general, although the particle size in the nanocomposite decreased compared to that in pure ZnO samples, the DLS data also indicate severe agglomeration of the primary nanoparticles in suspension, which is a critical factor for photocatalytic performance because it affects the active surface area.

To investigate the factors affecting photocatalytic properties, the Fe<sub>3</sub>O<sub>4</sub>/ZnO/CuO nanocomposites with different molar ratios in the MB solution were individually irradiated with UV and visible light for 20, 40, 60, 80, 100, and 120 minutes. Fig. 8 shows the absorption spectrum of MB before photocatalytic activity. The absorption rate of methylene blue is approximately 1.067 at 665 nm.

**Table 3.** Wavelength values of the absorption edge and the energy of the band gap of ZnO and Fe<sub>3</sub>O<sub>4</sub>/ZnO/CuO nanocomposites

Sample	Wavelength of absorption edge (nm)	Energy of the band gap (eV)
ZnO	382.16	3.24
Fe <sub>3</sub> O <sub>4</sub> /ZnO/CuO (1:1:0.3)	384.1	3.22
Fe <sub>3</sub> O <sub>4</sub> /ZnO/CuO (1:1:0.5)	386.31	3.20
Fe <sub>3</sub> O <sub>4</sub> /ZnO/CuO (1:1:1)	389.26	3.18
Fe <sub>3</sub> O <sub>4</sub> /ZnO/CuO (1:1:3)	398.54	3.11

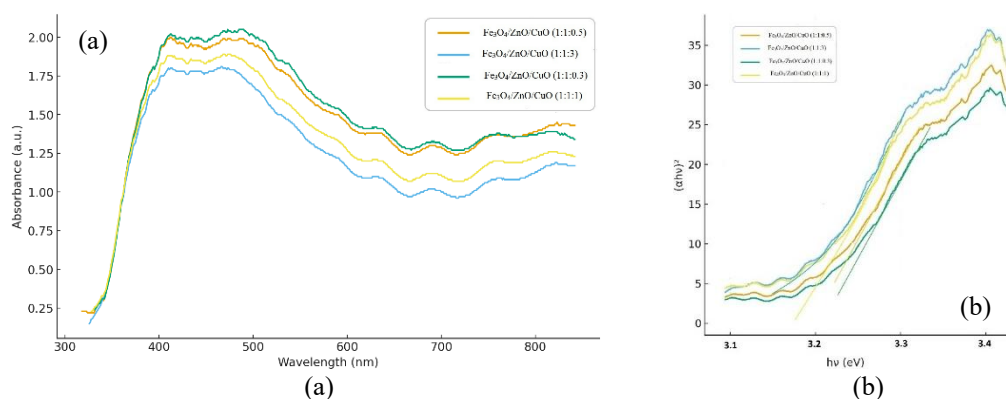


**Fig. 6.** Bandgap analysis curves of Fe<sub>3</sub>O<sub>4</sub>/ZnO/CuO nanocomposite: a) UV-VIS Absorption Spectra, b) Tauc's plots graphs ( $n = 2$ )

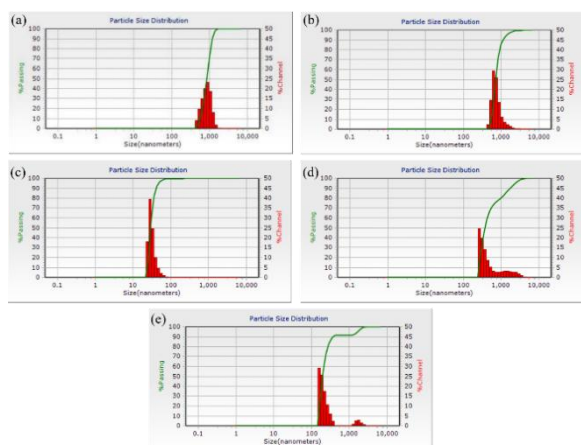


**Fig. 7.** DLS Analysis Results of  $\text{Fe}_3\text{O}_4/\text{ZnO}/\text{CuO}$  nanocomposites, a) ZnO, b)  $\text{Fe}_3\text{O}_4/\text{ZnO}/\text{CuO}$  (1:1:0.3), c)  $\text{Fe}_3\text{O}_4/\text{ZnO}/\text{CuO}$  (1:1:0.5), d)  $\text{Fe}_3\text{O}_4/\text{ZnO}/\text{CuO}$  (1:1:1), e)  $\text{Fe}_3\text{O}_4/\text{ZnO}/\text{CuO}$  (1:1:3)

The reduction of this amount in the presence of  $\text{Fe}_3\text{O}_4/\text{ZnO}/\text{CuO}$  nanocomposite and ZnO samples under visible and UV radiation reflects the color of this industrial dye. It demonstrates the nanocomposite's ability to treat industrial wastewater.

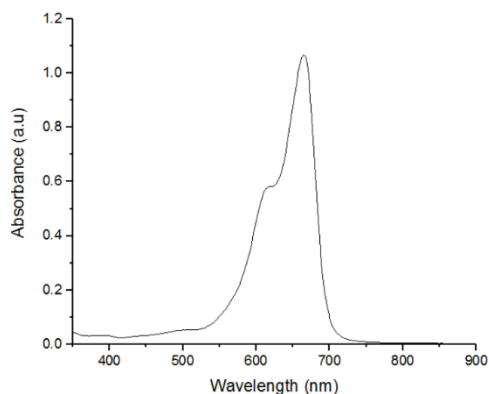
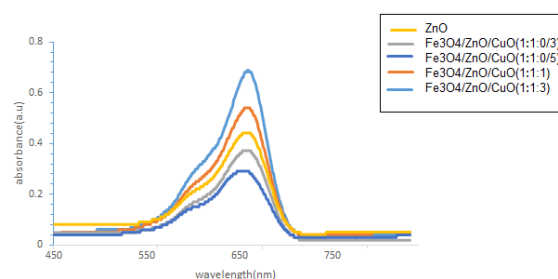


**Fig. 8.** Absorption spectrum of methylene blue before photocatalytic activity

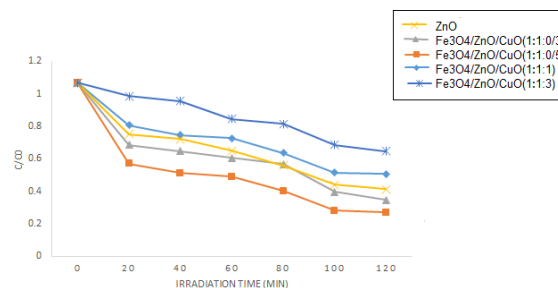
Fig. 9 shows the results of the photocatalytic activity under UV irradiation for over 120 minutes. The methylene blue absorption peak, initially at 0.005 g/L, decreased in each sample after 120 min. The amount of methylene blue removed by the  $\text{Fe}_3\text{O}_4/\text{ZnO}/\text{CuO}$  samples with a molar ratio of 1:1:0.5 is higher than that of other samples. The photocatalytic activity of samples is 58.76%, 65.32%, 72.82%, 49.39%, and 35.33% for ZnO,  $\text{Fe}_3\text{O}_4/\text{ZnO}/\text{CuO}$ , with molar ratios of 1:1:0.3, 1:1:0.5, 1:1:1, 1:1:3 respectively, which were calculated using the formula.

Fig. 10 illustrates a comparative diagram of the photocatalytic performance of  $\text{Fe}_3\text{O}_4/\text{ZnO}/\text{CuO}$

nanocomposites with different amounts of CuO under UV irradiation for 20 to 120 minutes. Under UV irradiation,  $\text{Fe}_3\text{O}_4/\text{ZnO}/\text{CuO}$  nanocomposites with 1: 1: 1 and 1: 1: 3 molar ratios have lower photocatalytic activity than pure ZnO. The shift of the absorption edge towards the visible spectrum and the reduction in the nanocomposites' band gap can be attributed to the incorporation of CuO. Due to the differences between the UV wave energy and the amount of energy needed to transfer electrons from the valence band to the conduction band in  $\text{Fe}_3\text{O}_4/\text{ZnO}/\text{CuO}$  nanocomposites, and the low efficiency of electron-cavity generation compared to ZnO, the above nanocomposites exhibit less photocatalytic activity.



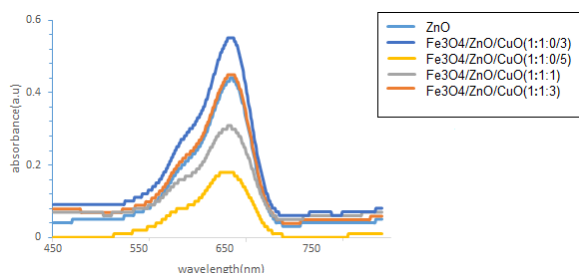
**Fig. 9.** Photocatalytic activity of  $\text{Fe}_3\text{O}_4/\text{ZnO}/\text{CuO}$  nanocomposites under UV radiation



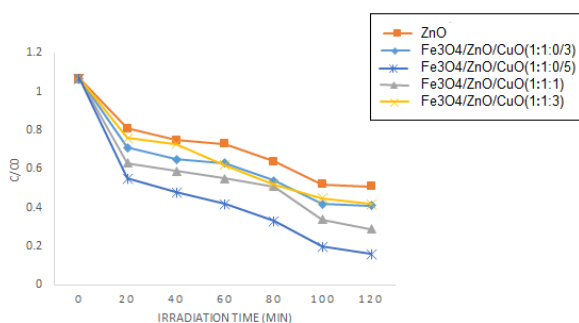
**Fig. 10.** Comparative diagram of  $\text{Fe}_3\text{O}_4/\text{ZnO}/\text{CuO}$  nanocomposites' photocatalytic efficiency under UV radiation

Fig. 11 shows the results of the photocatalytic activity under visible irradiation for over 120 minutes. The  $\text{Fe}_3\text{O}_4/\text{ZnO}/\text{CuO}$  composite with a 1:1:0.5 molar ratio demonstrated superior methylene blue dye removal compared to other samples. The photocatalytic degradation efficiencies were measured at 48.45% for pure ZnO, and for  $\text{Fe}_3\text{O}_4/\text{ZnO}/\text{CuO}$  composites: 62.27% at 1:1:0.3 ratio, 88.7% at 1:1:0.5 ratio, 77.94% at 1:1:1 ratio, and 57.82% at 1:1:3 ratio. Fig. 12 shows a comparative diagram of the photocatalytic activity of  $\text{Fe}_3\text{O}_4/\text{ZnO}/\text{CuO}$  nanocomposites with varying amounts of CuO under visible irradiation for 20-120 minutes.

The  $\text{Fe}_3\text{O}_4/\text{ZnO}/\text{CuO}$  nanocomposite with a 1:1:0.5 molar ratio exhibits the best photocatalytic activity. However, the photocatalytic activity of the samples improved relative to pure ZnO, indicating that the  $\text{Fe}_3\text{O}_4/\text{ZnO}/\text{CuO}$  nanocomposites exhibit higher activity in the visible light range.



**Fig. 11.** Photocatalytic activity of  $\text{Fe}_3\text{O}_4/\text{ZnO}/\text{CuO}$  nanocomposites under visible radiation



**Fig. 12.** Comparative diagram of photocatalytic efficiency of  $\text{Fe}_3\text{O}_4/\text{ZnO}/\text{CuO}$  nanocomposites under visible radiation

To investigate the influence of ultrasound on the photocatalytic activity of the  $\text{Fe}_3\text{O}_4/\text{ZnO}/\text{CuO}$  nanocomposites with different molar ratios, the nanocomposites were irradiated with ultrasonic and visible light for 20-120 minutes in a methylene blue solution, and their photocatalytic activity was measured. Fig. 13 illustrates this. The results showed that the  $\text{Fe}_3\text{O}_4/\text{ZnO}/\text{CuO}$  nanocomposites with a 1:1:3 molar ratio exhibit the highest photocatalytic activity under ultrasound and visible light irradiation. The enhanced performance can be attributed to CuO's appropriate bandgap. Under ultrasonic conditions, CuO showed a higher activation energy than ZnO, and increasing its content improved photocatalytic activity. As illustrated in Fig. 13, complete photocatalytic degradation (100% efficiency) was achieved after 120 minutes of treatment. The  $\text{Fe}_3\text{O}_4/\text{ZnO}/\text{CuO}$  nanocomposites with different molar ratios were investigated under UV, visible, and ultrasonic waves, and their comparative results are shown in Fig. 14. Enhancing photocatalytic

activity of the nanocomposite under visible light and ultrasonic by increasing CuO content is mainly attributed to the narrow band gap of CuO, which enables strong visible-light absorption and promotes efficient charge separation through the formation of the n-p heterojunction. In this procedure, CuO acts as an effective electron trap, repressing recombination and enhancing the generation of reactive species. Under ultrasonic-visible light, the highest efficiency was observed, which can be attributed to two factors. Firstly, Ultrasonic increases the production of active radicals for photocatalytic activity and also improves the organic transfer of colour at the catalyst surface. Secondly, the deagglomeration of photocatalyst particles by ultrasonication increases the specific surface area. The ultrasonic process operates via cavitation, which forms holes, leading to elevated temperature and pressure in the reaction medium. This process involves the formation, gradual growth, and eventual bursting of a series of bubbles by sonication. Under such conditions, hot spots form that can convert water molecules into active hydroxyl radicals and hydrogen peroxide, which then destroy toxic compounds.

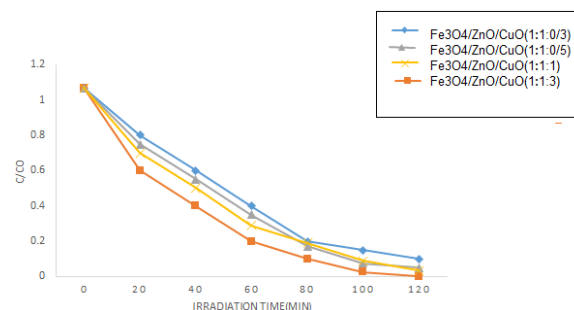


**Fig. 13.** Comparative diagram of photocatalytic efficiency of  $\text{Fe}_3\text{O}_4/\text{ZnO}/\text{CuO}$  nanocomposites under visible and ultrasound radiation

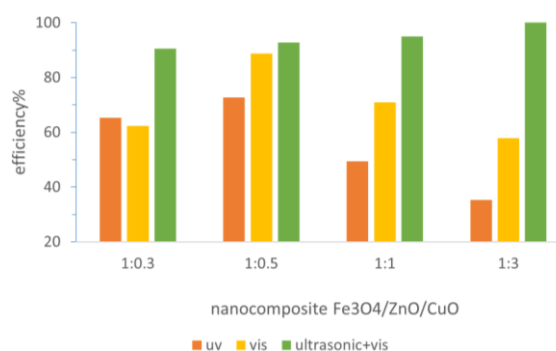


**Fig. 14.** Comparative diagram of photocatalytic efficiency of  $\text{Fe}_3\text{O}_4/\text{ZnO}/\text{CuO}$  nanocomposites under UV, visible, and ultrasonic radiation

Based on other related research, the stability of the catalysts under light and ultrasonic irradiation was evaluated using the same batch of nanocomposites for four cycles, with the same amount of fresh MB solution added after each run. The results in Fig. 15 show that the catalysts exhibit good stability and magnetic recyclability from the treated solutions after successive degradation reactions. The XRD and FTIR measurements were also performed on the catalysts after multiple cycles, and compared with the results obtained before the reaction. In Fig. 15(a), all XRD peaks corresponding to cubic spinel, hexagonal wurtzite, and monoclinic structures remained at the same values after four cycles. So, there is no change in the crystalline structure.

The same conclusion is drawn from the IR absorption measurements because the IR peaks of the functional groups remain unchanged after photocatalytic degradation, Fig. 15(b) [30].

Various factors, such as electron generation, electron trapping, charge-carrier recombination, the average crystal size, and the band gap energy, are important for understanding the photocatalyst mechanism. The varying molar proportions of CuO in the samples significantly influence the photocatalytic mechanism. Research has shown that a larger specific surface area creates more active surface sites, reducing interfacial charge-carrier transfer resistance and enhancing photocatalytic performance. The nanocomposites exhibit distinct patterns of photocatalytic performance under visible light versus UV radiation.

Diffuse reflectance spectroscopy analysis revealed that ZnO has a band gap of 3.24 eV, while CuO has a band gap of 1.54 eV [30]. As an n-type

semiconductor, ZnO's electrons in the valence band become excited and move to the conduction band when exposed to UV radiation, which is possible due to its specific band gap energy. In contrast, CuO, a p-type semiconductor, can facilitate electron transfer from the valence to the conduction band upon visible light exposure. The complementary band-gap energies of ZnO, CuO, and Fe<sub>3</sub>O<sub>4</sub> can facilitate electron transfer between these materials. When exposed to visible light, CuO generates electron-hole pairs due to its favourable band gap. Additionally, electrons from ZnO's valence band, which have lower energy than its conduction band, can move into structural defects such as oxygen vacancies. When CuO's excited electrons migrate to ZnO's conduction band, they can interact with Fe<sup>3+</sup> to form Fe<sup>2+</sup> ions. These unstable Fe<sup>2+</sup> ions then react with oxygen molecules to generate superoxide radicals. Simultaneously, holes created in ZnO's valence band can either transfer to CuO's valence band or interact with water molecules to create OH<sup>•</sup>. Additionally, holes in CuO can generate hydroxyl radicals through interaction with water. Under UV light, the capture of electrons by Fe<sup>3+</sup> ions enhances the probability of hole-mediated hydroxyl radical formation, which then breaks down organic pollutants. During this process, electrons from ZnO's valence band are excited exclusively to its conduction band, leaving holes in the valence band. These excited electrons are captured by Fe<sup>3+</sup> ions, forming Fe<sup>2+</sup> ions that produce superoxide radicals. Concurrently, the photogenerated holes react with water molecules to form OH<sup>-</sup> radicals, which are the key agents in decomposing methylene blue during the catalytic reaction [26-28].

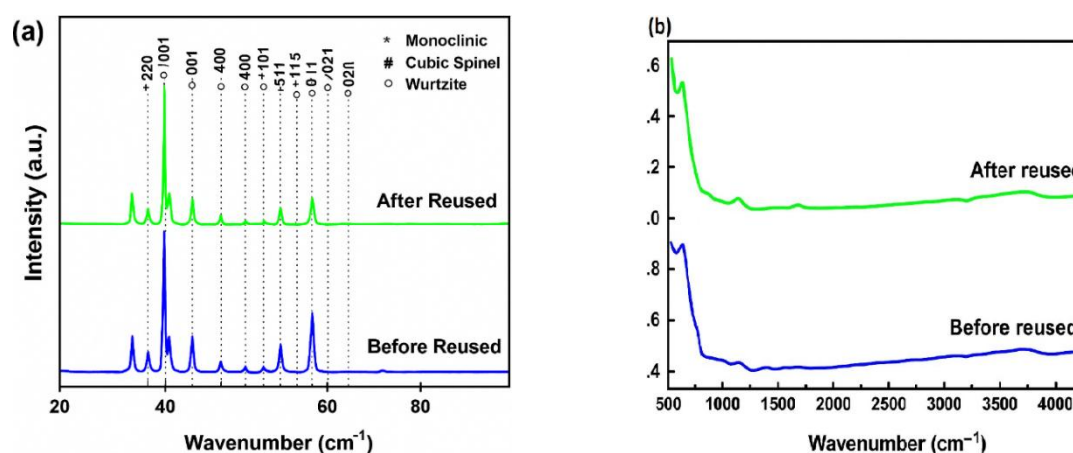


Fig. 15. a) XRD patterns of Fe<sub>3</sub>O<sub>4</sub>/ZnO/CuO nanocomposites before reused, b) IR peaks of Fe<sub>3</sub>O<sub>4</sub>/ZnO/CuO nanocomposites after and before reused [30]

The mechanism behind MB degradation using ultrasonic treatment has been verified. When ultrasonic waves are applied, they induce acoustic cavitation, generating extreme conditions of temperature (5000 K) and pressure (1000 atm). This process produces light across a broad wavelength spectrum (sonoluminescence), activating both ZnO and CuO semiconductors and forming electron-hole pairs [28]. These electron-hole pairs contribute to MB degradation through the same mechanisms observed in photocatalysis.

When exposed to both visible light and ultrasound, CuO shows enhanced activation due to its suitable band gap energy. This explains why the nanocomposite containing the highest proportion of CuO ( $\text{Fe}_3\text{O}_4/\text{ZnO}/\text{CuO}$  in a 1:1:3 molar ratio) demonstrates superior photocatalytic performance under visible-light conditions. Moreover, the extreme temperature and pressure conditions created by ultrasound in aqueous environments promote the direct formation of  $\text{OH}^\cdot$  radicals through Fenton reactions [29]:



According to Yuan and colleagues' research [30], the  $\text{H}_2\text{O}_2$  produced (as shown in Eq. 7) can interact with  $\text{Fe}^{2+}$  to generate  $\text{OH}^\cdot$  radicals and  $\text{Fe}^{3+}$  ions. The increased production of  $\text{OH}^\cdot$  radicals through various pathways under ultrasonic irradiation results in improved degradation efficiency.

The reason that the ternary nanocomposite with the ratio of 1:1:0.5 is optimal under visible light, while 1:1:3 is best under sonolysis, is attributed to the narrow band gap of CuO, which enables strong visible-light absorption and promotes efficient charge separation through the formation of the n-p heterojunction. In this procedure, CuO acts as an effective electron trap, repressing recombination and enhancing the generation of reactive species. In contrast, under UV irradiation, increasing the ratio of CuO in the nanocomposite reduces the photocatalytic performance because CuO does not absorb UV efficiently and partially covers the surface of the primary semiconductor (reducing the specific interface areas). Also, agglomeration occurs as the CuO content increases, which limits UV absorption. Moreover, extra CuO can behave as recombination centers, accelerating electron-hole recombination and lowering the overall photocatalytic activity.

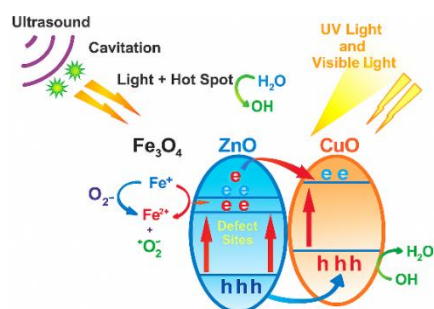


**Fig. 16.** Schematic of the photocatalytic mechanism of  $\text{Fe}_3\text{O}_4/\text{ZnO}/\text{CuO}$  nanocomposites

#### 4. CONCLUSIONS

In conclusion, the  $\text{Fe}_3\text{O}_4/\text{ZnO}/\text{CuO}$  nanocomposites were successfully synthesised via sol-gel synthesis. The degradation of methylene blue was examined under both light and ultrasonic irradiation to analyse the photocatalytic activity. Results revealed that ultrasonic treatment played a crucial role, significantly improving the photocatalytic performance of the nanocomposite materials. The optimal composition of the photocatalyst nanocomposite material was investigated through structural characterization using various techniques. SEM images showed that the nanocomposite exhibited a cauliflower-like structure, with particle sizes ranging from 25.3 to 57.08 nm, as measured using ImageJ. EDX analysis also confirmed improved dispersion of the samples. Additionally, dot mapping of the nanocomposite structure indicated that the elements were uniformly distributed throughout the material. Dynamic Light Scattering (DLS) results showed that increasing the copper oxide content in the  $\text{Fe}_3\text{O}_4/\text{ZnO}/\text{CuO}$  nanocomposite led to a reduction in particle size distribution. Moreover, the addition of CuO decreased the band gap energy, shifting light absorption toward the visible region. The photocatalytic performance revealed 100% degradation of MB for  $\text{Fe}_3\text{O}_4/\text{ZnO}/\text{CuO}$  nanocomposite at a 1:1:3 molar ratio under ultrasound and visible light after 120 minutes. Additionally, the use of an external magnet allowed for easy separation and recovery of the nanocomposite from the solution after the reaction. These findings highlight the effectiveness of the ternary  $\text{Fe}_3\text{O}_4/\text{ZnO}/\text{CuO}$  nanocomposite catalyst in removing organic pollutants from wastewater.

#### ACKNOWLEDGEMENTS

The authors gratefully acknowledge the mechanical faculty of Tabriz University and the laboratory of

the Materials Science and Engineering Department of Tabriz University.

## REFERENCES

- [1] Zhu, L.; Zhou, Y.; Fei, L.; Cheng, X.; Zhu, X.; Deng, L.; Ma, X. "Z-scheme CuO/Fe<sub>3</sub>O<sub>4</sub>/GO heterojunction photocatalyst: Enhanced photocatalytic performance for elimination of tetracycline". *Chemosphere* 2022, 309 (Pt 2), 136721.
- [2] Alzuabidi, H. A.; Naghipour, A.; Fardood, S. T. "Green synthesis and characterization of Cu<sub>0.5</sub>Zn<sub>0.5</sub>FeAlO<sub>4</sub> magnetic nanoparticles with enhanced photocatalytic activity". *J. Ultrafine Grained Nanostruct. Mater.* 2024, 158–167.
- [3] Hu, Y.; Jensen, L.; Schatz, G. "Photocatalytic reaction pathways on TiO<sub>2</sub> surfaces: a theoretical study". *J. Am. Chem. Soc.* 2006, 128, 15734–42.
- [4] Ge, M.; Cao, C.; Huang, J.; Li, S.; Chen, Z.; Zhang, K.; et al. "A review of one-dimensional TiO<sub>2</sub> nanostructured materials for environmental and energy applications". *Mater. Chem. A* 2016, 4, 6772–6801.
- [5] Asghar, A.; Aziz, A.; Mohd, A. "Advanced oxidation processes for in situ production of hydrogen peroxide/hydroxyl radical for textile wastewater treatment: a review". *J. Cleaner Prod.* 2015, 87, 826–38.
- [6] Shakir, A. K.; Ghanbari-Adivi, E.; Baron, A. S.; Soltani, M. "Investigation of the Effect of Calcination Time on the Antibacterial, Antifungal and Anticancer Activities of TiO<sub>2</sub>/ZnO Nanocomposites". *Iran. J. Mater. Sci. Eng.* 2025, 22 (1).
- [7] Safavi, M. S.; Bozorg, S.; Ahadzadeh, I.; Safavi, M. S. "Development of heterogeneous nano-zeolite catalyzing Fenton-like oxidation processes for metalworking fluid wastewater treatment: A comparison with conventional methods". *J. Ultrafine Grained Nanostruct. Mater.* 2024, 190–202.
- [8] Asai, M. M.; Tapadia, K. "Biofabricated magnetic CuO@Fe<sub>3</sub>O<sub>4</sub> nanocomposites: Synthesis, characterization and Brilliant Green dye removal from aqueous media and its kinetics study". *J. Indian Chem. Soc.* 2025, 102 (5), 10166.
- [9] Ajmal, A.; Majeed, I.; Malik, R.; Idriss, H.; Nadeem, M. "Principles and mechanisms of photocatalytic dye degradation on TiO<sub>2</sub>-based photocatalysts: a comparative overview". *RSC Adv.* 2014, 4, 37003–26.
- [10] Soleimani-Amiri, S.; Hossaini, Z.; Azizi, Z. "Synthesis and investigation of biological activity of new oxazinoazepines: Application of Fe<sub>3</sub>O<sub>4</sub>/CuO/ZnO@MWCNT magnetic nanocomposite in reduction of 4-nitrophenol in water". *Polycycl. Aromat. Compd.* 2023, 43 (4), 2938–59.
- [11] Cruz, M.; Gomez, C.; Duran-Valle, C.; Pastrana-Martinez, L.; Faria, J.; Silva, A.; et al. "Bare TiO<sub>2</sub> and graphene oxide TiO<sub>2</sub> photocatalysts on the degradation of selected pesticides and influence of the water matrix". *Appl. Surf. Sci.* 2015, 268, 1–9.
- [12] Rahmat, R.; Heryanto, H.; Ilyas, S.; Fahri, A. N.; Mutmainna, I.; Rahmi, M. H.; Tahir, D. "The relation between structural, optical, and electronic properties of composite CuO/ZnO in supporting photocatalytic performance". *Desalination Water Treat.* 2022, 270, 289–301.
- [13] Shen, Y.; Wang, Y.; Chen, Y.; Park, J. K.; Fang, S.; Feng, K. "Synthesis of Fe<sub>3</sub>O<sub>4</sub>/CuO/ZnO/RGO and its catalytic degradation of dye wastewater using dielectric barrier discharge plasma". *Arab. J. Chem.* 2023, 16 (4), 104571.
- [14] Ohtani, B. "Photocatalysis A to Z – What we know and what we do not know in a scientific sense". *J. Photochem. Photobiol. C* 2008, 11, 157–78.
- [15] Rashid, H.; Muhammad, E.; Hassan, M.; Rauf, A.; Bashir, A.; Ali, W.; et al. "Synthesis, structural and photocatalytic properties of ZnO-CuO, ZnO-Graphene and ZnO-CuO-Graphene nanocomposites". *Polyhedron* 2025, 273, 117471.
- [16] Li, X.; Liu, J.; Liu, E.; Wan, J.; Bai, Z. "A review of heterogeneous photocatalysts for environmental remediation: materials and processes". *Chemosphere* 2016, 172, 124–40.
- [17] Takahashi, M.; Okada, K.; Malfatti, L.; Innocenzi, P. "Formation of interfaces responsive and adaptive to environment via the sol-gel method". *J. Sol-Gel Sci. Technol.* 2024, 112 (1), 174–81.
- [18] Malhotra, A.; Saini, A.; Jindal, N.; Kumar, R. "Combustion synthesized Fe<sub>3</sub>O<sub>4</sub>/α-Fe<sub>2</sub>O<sub>3</sub>/C nanocomposites for efficient radiative and non-radiative degradation of methylene

- blue dye". *Inorg. Chem. Commun.* 2025, 173, 113808.
- [19] Bopape, D. A.; Hintscho-Mbita, N. C. "Commelina benghalensis-mediated CuO–ZnO nanocomposite: Effect of the pn heterojunction on the photocatalytic activity against Congo red and carbamazepine". *Inorg. Chem. Commun.* 2025, 154, 114529.
- [20] Intharaksa, O.; Nanan, S.; Patdhanagul, N.; Panphojan, T.; Srikakul, T.; Tantisuwichwong, N.; et al. "Preparation of magnetic CuO/Fe<sub>3</sub>O<sub>4</sub>/ZnO photocatalyst for complete degradation of methylene blue under natural sunlight irradiation". *J. Phys. Chem. Solids* 2023, 182, 111577.
- [21] Melese, A.; Wubet, W.; Abebe, A.; Hussien, A. "A comprehensive review on recent progress in synthesis methods of ZnO/CuO nanocomposites and their biological and photocatalytic applications". *Results Chem.* 2025, 7, 102141.
- [22] Wahba, M. A.; Yakout, S. M. "Microwave-synthesized ZrO<sub>2</sub>/ZnO heterostructures: fast and high charge separation solar catalysts for dyes-waste degradation". *J. Sol-Gel Sci. Technol.* 2022, 104 (2), 330–41.
- [23] Ross, J. R. H. "Catalyst characterization". In *Contemporary Catalysis Fundamentals and Current Applications*; 2019; Chapter 5, pp 121–132.
- [24] Chen, X.; Selloni, A. "Introduction: Titanium dioxide (TiO<sub>2</sub>) nanomaterials". *Chem. Rev.* 2014, 114, 9281–82.
- [25] Etay, H.; Kumar, A.; Yadav, O. P. "Kinetics of photocatalytic degradation of methylene blue dye in aqueous medium using ZnO nanoparticles under UV radiation". *J. Anal. Pharm. Res.* 2023, 12 (1).
- [26] Asli, S. A.; Taghizadeh, M. "Sonophotocatalytic degradation of pollutants by ZnO-based catalysts: A review". *Chem. Select* 2020, 13720–73.
- [27] Benamara, M.; Nassar, K. I.; Essid, M.; Frick, S.; Rugmini, R.; Sekhar, K. C.; Silva, J. P. "Visible light-driven removal of Rhodamine B using indium-doped zinc oxide prepared by sol–gel method". *J. Sol-Gel Sci. Technol.* 2024, 111 (2), 553–65.
- [28] Yuan, N.; Zhang, G.; Guo, S.; Wan, Z. "Enhanced ultrasound-assisted degradation of methyl orange and metronidazole by rectorite-supported nanoscale zero-valent iron". *Ultrason. Sonochem.* 2016, 28, 62.
- [29] Khan, M. A. N.; Siddique, M.; Wahid, F.; Khan, R. "Removal of reactive blue 19 dye by sono, photo and sonophotocatalytic oxidation using visible light". *Ultrason. Sonochem.* 2015, 26, 370–77.
- [30] Taufik, A.; Saleh, R. "Synthesis of iron (II, III) oxide/zinc oxide/copper (II) oxide(Fe<sub>3</sub>O<sub>4</sub>/ZnO/CuO) nanocomposites and their photo sonocatalytic property for organic dye removal". *J. Colloid Interface Sci.* 2017, 491, 27–36.